Journal of Applied Fluid Mechanics, Vol. 17, No. 9, pp. 1792-1805, 2024.
Available online at www.jafmonline.net, ISSN 1735-3572, EISSN 1735-3645.
https://doi.org/10.47176/jafm.17.9.2487

Distribution of the Velocity Profile via Analytical and Three-Dimensional Numerical Vegetation Modeling

A. A. Hussain[1,2], M. A. Al-Obaidi [3,4, †], A. S. Mohammed[5], Y. M. John[6] and F. L. Rashid [7]

[1] *Department of Mechanical Engineering, Faculty of Engineering and Informatics, University of Bradford, Bradford, BD7 1DP, UK*
[2] *Department of Engineering and Construction, Faculty of Engineering and Construction, Bradford College, Bradford, BD7 1QX, UK*
[3] *Technical Institute of Baquba, Middle Technical University, Baghdad 10074, Iraq*
[4] *Technical Instructor Training Institute, Middle Technical University, Baghdad 10074, Iraq*
[5] *Civil Engineering Department, College of Engineering, University of Sulaimani, Iraq*
[6] *Department of Chemical Engineering, Faculty of Engineering and Informatics, University of Bradford, Bradford, BD7 1DP, UK*
[7] *Petroleum Engineering Department, College of Engineering, University of Kerbala, Karbala 56001, Iraq*

[†]*Corresponding Author Email: dr.mudhar.alaubedy@mtu.edu.iq*

ABSTRACT

Understanding the ecological conditions of vegetation growth in water sources is vital to appraise the influence of vegetation on river engineering. Based on the experimental information that is accessible, the consequences of vegetation on flow resistance is described as an alteration in the drag coefficient and the planned area. The current study analytically estimates the vertical distribution of stream-wise velocity in open-channel flow while considering rigid and flexible vegetation. The flow is vertically separated into top free water layer and bottom vegetation layer using the projected deflection height of both vegetation. Related momentum calculations for each layer are then derived. Based on the gathered experimental data, a 3D numerical model with various simulation situations is used to model, calibrate, and evaluate the artificial cylinders. A considerable deflection analysis is utilised to calculate the velocity-dependent stem height. This has proven to be more precise compared to formerly deflection investigation. The estimated outcomes show that precise predictions may be made for the vertical contours of vertical Reynolds shear stress based on mean horizontal velocity. The numerical simulations demonstrate that plant flexibility reduces the vertical Reynolds shear stress and prompted flow resistance force of the vegetation.

Article History

Received December 8, 2023
Revised March 30, 2024
Accepted April 5, 2024
Available online July 2, 2024

Keywords:

Open-channel flow
Analytical model
Numerical model
Velocity distribution
Ansys fluent
3D Simulation

1. INTRODUCTION

The presence of vegetation within river systems is beneficial to their environmental functions. It impacts flow conditions by enhancing increasing water purification due to increasing the flow resistance. Referring to Rowiński and Kubrak (2002), the foregoing research effectively modified their analytical model for several kinds of rigid developing vegetation, and flexible sub-merged vegetation (Kubrak et al., 2008; Kubrak et al., 2012), interpreting the vegetation resistance in open-channel flows in an alternate manner (Anjum and Tanaka, 2020). Some successful examples of numerical models that investigated the sub-merged vegetation in open channel flow are discussed below.

Fischer-Antze et al. (2001) used a 3D model, velocity distributions in open-channels that are partially vegetated have been calculated. The k-turbulent model were used for resolving the Navier-Stokes equations while modeling the vegetation by means of vertical cylinders. Navier-Stokes equations include a sink element that containe a correlation for the drag force on the plants. Three laboratory trials were used to compare the numerical model against the developed model to validate the results. In each example, there were differences in the vertical and horizontal velocities and vegetation densities. Also included in the experiments were various cross-sectional forms. In all tests, the calculated and actual velocity profiles showed an accepted degree of agreement.

The hydraulic influence of willow stands on the velocity distribution was addressed by Wilson et al. (2006). Accordingly, a simulation of the hydraulic resistance of willow stands discretely from the bed resistance was made. This method used to mimic two

flood occurrences with variable magnitudes and plant development stages. The estimated velocity contours were found to significantly differ depending on whether the willow stands were modeled as bending or vertical. When the plants are modeled vertically as opposed to in high degrees of bending, it is discovered that the effect of utilising a drag force method constructed on an irregular subjected area distribution is stronger.

Erduran and Kutija (2003) analysed and formulated the drag effects caused by plants through numerical and experimental studies. The authors suggested a quasi 3D numerical method. They combined the Navier Stokes formula for vertical velocity distributions finite difference with the finite-volume solutions of the two dimensional shallow water correlations. Both sets of equations take the drag forces into consideration.

Using the Flow-3D, Ren et al. (2021) studied the effects of the vertical velocities and longitudinal transverse on the flow velocity. An evaluation of sensitivity was carried out for the height and diameter of vegetation, and flowrate after verification using experimental measurements. It was concluded that the diameter of vegetation has a greater influence on the flow velocity when the longitudinal velocity is high. However, the vertical distribution's inflection point is identified by the height of the vegetation.

Based on gathered experimental data, a regression analysis has been conducted by Hussain et al. (2023) to develop an explicit formula to guesstimate the drag coefficient of rigid vegetation under emergent and sub-merged flow circumstances. Considering an analogy with the log wake law, the formula offers an indicator of length measure that standardizes the velocity contours of the open-channel flow considering sub-merged rigid vegetation. The formula was created by conducting a regression analyses on each parameter, comprising the vegetation density, sub-merged ratio, and Re numbers, while taking into account the Froude number ranges for the water flows and the flows via vegetated channel.

This study intends to develop a three-dimensional mathematical technique for estimating bulk flow velocity for both rigid and flexible vegetation under sub-merged flow cases. In this regard, the model predicts analytically the vertical distribution of stream-wise velocity in open-channel flow while considering the rigid and flexible vegetation. Several tests are conducted to simulate the outcomes of rigid vegetation in a typical open-channel considering totally sub-merged vegetation.

2. APPLIED METHODOLOGIES

The applied methodologies used in this research have relied on numerical and analytical models to evaluate how the existence of vegetation affects flow resistance in open-channel flows. 3D CFD models relying on Reynolds average Navier Stokes (RANS) used the performing strategy technique to evaluate the analytical model and produce precise flow estimations (Fig. 1). The mathematical models have been successfully evaluated against the gathered data and utilised to forecast the

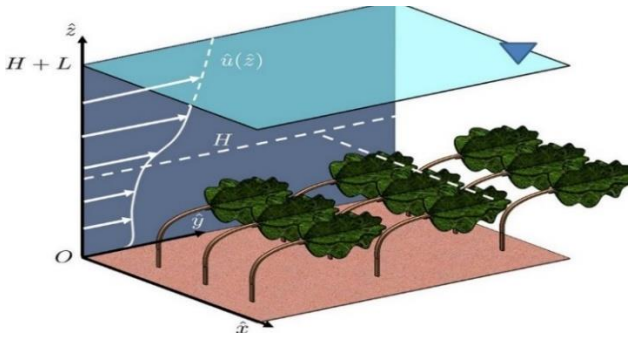

Fig. 1 Concept of the vegetation model (Rowiński and Kubrak, 2002)

averaged flow velocity and resistance coefficient employing artificial cylinders for the velocity contour.

In a vegetated layer flow for flexible and rigid vegetation (Fig. 2), the developed analytical model has considered the deflection point based on the cantilever beam theory. This aids to demonstrate the velocity contours in the mixing-layer region between the vegetation layer and the free water surface layer for sub-merged vegetation stems. Referring to Wilson et al. (2006), who noted increased streamwise velocities in the vegetation layer owing to significant drag, a flow movement in both the upstream and downstream directions happened at the places situated behind both flexible and stiff plant stems. The flow structures around vegetation stems were demonstrated by the numerical results, This is more easily observed in the reflected data, as these can be challenging to see with experimental observations, as illustrated by Fischer-Antze et al. (2001). The current investigation focused on the turbulence flow in an open-channel with artificial vegetation stems that were represented by a sequence of rigid cylinders of a small-diameter that extended vertically from bed of the channel. In this study, CFD finite-volume procedure was used to perform the three dimensions computations.

The equation for momentum and the mathematical formulas of the adapted model k-ε are considered in the numerical model employed to determine the average velocities and the features of turbulence flow.

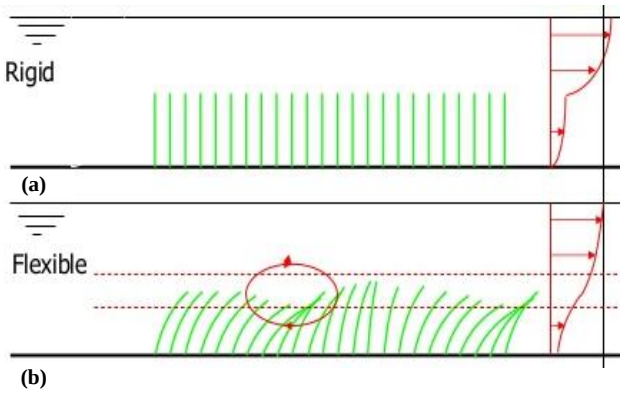

Fig. 2 (a) Rigid and (b) Flexible vegetation stems (Kubrak et al., 2008)

The boundary conditions have been considered in the channel axis direction and employed to lessen the computational overhead (Jiménez-Hornero et al. 2007). Tetrahedral elements have been used to discretize the computational domain, which was accomplished by selecting a mesh that strikes a fair compromise between the solution's stability and the resolution of the flow field. Nevertheless, it takes a considerable computing power to achieve mesh independent solutions for complicated geometric issues as represented in the current study.

3. VELOCITY CONTOUR IN VEGETATION AND SURFACE LAYERS

3.1 Velocity Contour in Vegetation Layer

In this study, a large deflection of vegetation occurs due to the high flexibility of the stems and drag coefficient while considering both the wall boundary stress and bed are insignificant (Jiménez-Hornero et al., 2007; Hussain et al., 2023). As a result, Ghisalberti and Nepf (2004) and Tang et al. (2014) identified the momentum formula of a steady, fully established, one dimensional vegetated flow, as follows.

$$\frac{\partial \tau(z)}{\partial z} = F_D(z) - \rho g i \tag{1}$$

τ, z, and ρ are the shear-stress (kg/ms^2), vertical co-ordinate (m), and density of water (kg/m^3), respectively. g is the acceleration (m/s^2), and i is the energy gradient (-). Eq. 2 represents the drag force on vegetation

$$F_D(z) = \frac{1}{2} m\, D \rho C_D\, U_{(z)}^2 \tag{2}$$

C_D, m, and D are the drag coefficient (-), vegetation elements (1/m^2), and diameter stem vegetation element (m). The flow velocity in the z direction is U(z) (m/s).

The momentum problem is analytically solved using the Boussinesq principle, and the turbulent shear-stress is specifically calculated using the eddy viscosity principle

$$\tau(z) = \xi \frac{\partial u(z)}{\partial z} = \rho (C_p L u) \frac{\partial u}{\partial z} \tag{3}$$

ξ is the turbulent viscosity (kg/ms), C_p is the turbulent intensity factor and L is the scale length of vegetation. The vertical transmission of momentum is precisely ascertained by the length scale and velocity scale that combine to define $\tau(z)$. The flow velocity U(z) is supposed to correspond to the typical velocity scale as stated by Tsujimoto and Kitamura (1990). It is also presumed that the typical length scale (α) has no dependence of z-dimension. The turbulence shear stress is depicted in the counter of Eq. 4

$$\tau(z) = a\, \rho\, u(z) \frac{\partial u(z)}{\partial z} \tag{4}$$

Eq. 3 can then be written in the form of Eq. 5

$$u(z).\frac{\partial^2 u(z)}{\partial z^2} + \left(\frac{\partial u(z)}{\partial z}\right)^2 = \frac{m\, D \rho C_D U^2(z)}{2\, a} - \frac{g\, i}{a} \tag{5}$$

The mathematical integration can introduce an analytical solution of Eq. 5 as follows;

$$u(z) = \sqrt{C_1 e^{-\sqrt{2A}z} + C_2 e^{\sqrt{2A}z} + U_{s0}^2} \qquad (0 < z < h_v) \tag{6}$$

h_v denotes the vegetation height (m). Also,

$$A = \frac{m\, D\, C_D}{2\, a} \tag{7}$$

The distinctive fixed flow velocity in non-sub-merged vegetation (U_{s0}) can be represented as stated by Baptist et al. (2010).

$$U_{s0} = \sqrt{\frac{2\, g\, i}{C_D\, m\, D}} \tag{8}$$

U_{s0} tracks directly Eq. 6 while setting the velocity gradients at zero and considering the boundary conditions as C_1 and C_2. In this regard, the bottom shear-stress can be discarded at the bed of z = 0, and the flow velocity can be presumed to indicate U_{s0}. Furthermore, the boundary condition can be resolved by shear-stress for the case of the top of the vegetation layer

$$\tau(h_v) = \rho\, g\, i\, (H - h_v) \tag{9}$$

H and hv represent the water depth (m) and vegetation height (m), respectively. The mathematical expressions of boundary conditions (C_1 and C_2) are represented in the following

$$C_1 = \frac{-2\, g\, i\, (H - h_v)}{a\sqrt{2A}\,(e^{h_v\sqrt{2A}} + e^{-h_v\sqrt{2A}})} \qquad C_2 = -\,C_1 \tag{10}$$

The above developed model has ascertained the established velocity contour of the vegetation layer. In this context, Tang et al. (2014) derived the mathematical expression of the characteristic length scale (α) as indicated in Eq. 11

$$\alpha = 0.0793\, h_v\, \mathrm{Ln}\left(\frac{H}{h_v}\right) - 0.0009 \quad (a \geq 0.001) \tag{11}$$

3.2 Velocity Contour in Surface Model Layer

The mixing length idea of Prandtl is accommodated by the surface layer caused in the familiar logarithmic flow velocity contour. The virtual bed of this contour appears to lie under that level from a distance (hs) but is not aligned with the top of the vegetation. Eq. 12 elucidates the flow velocity contour

$$u(z) = \frac{U_*}{K}\mathrm{Ln}\left(\frac{Z - (h_v - h_s)}{Z_0}\right) = \frac{U_*}{K}\mathrm{Ln}\left(\frac{Z - Z_m}{Z_0}\right) \quad (\mathrm{hv} < z < \mathrm{h}) \tag{12}$$

K is the fixed parameter of Von Karman, which equals 0.4. h_v and z_0 represent the distance between the virtual bed of surface layer and top of vegetation (m), and length scale of the surface layer's bed roughness (m), respectively. The following equation of Nepf and Vivoni (2008) can be demonstrated while considering equal values at the interface ($z=h_v$) of the actual and gradient flow velocity of vegetation and surface layer:

$$Z_m = (h_v - h_s) \tag{13}$$

Baptist et al. (2010) derived the turbulence shear stress while realising the following variables:

$$C_p L = \frac{(H - h_v)}{20} \tag{14}$$

$$L = \sqrt{\frac{C_p L}{a\, C_D}} \tag{15}$$

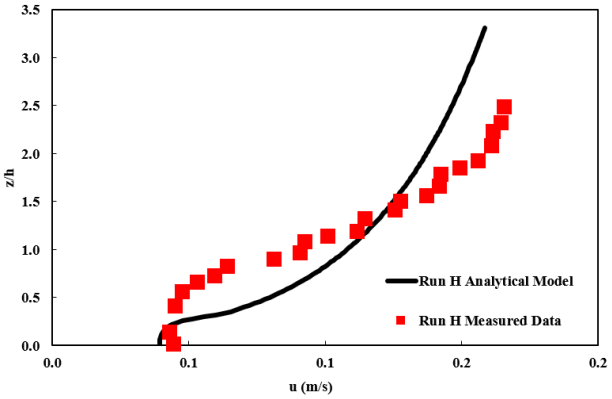

Fig. 3 Presentation of Run H

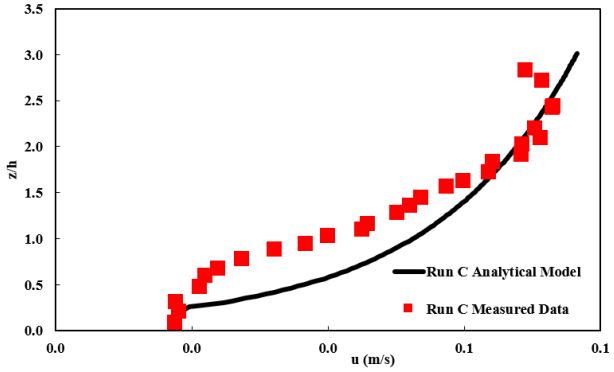

Fig. 5 Presentation of Run C

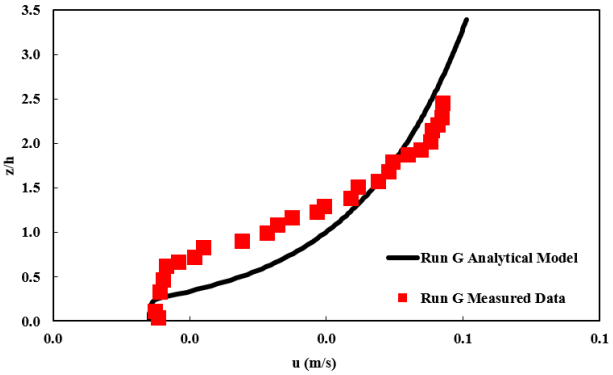

Fig. 4 Presentation of Run G

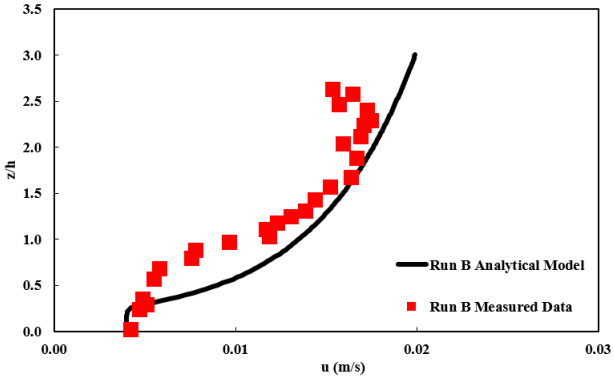

Fig. 6 Presentation of Run B

The above Boussinesq's eddy viscosity model was authorised against the associated data of Nepf and Vivoni (2008) and elaborated the following correlations of Z_0 and h_s as follows,

$$Z_0 = h_s e^{-K\sqrt{\frac{2L}{C_{PL}}\left(1+\frac{L}{H-h_v}\right)}} \tag{16}$$

$$h_s = L\left(1 - e^{\left(-\frac{h_v}{L}\right)}\right) \tag{17}$$

High deflection within the free water surface does not occur due to the free vegetation zone. Huai et al. (2013) developed a correlation for the shear velocity

$$U_* = \sqrt{g\, i\, (H - h_v)} \tag{18}$$

Numerous factors were considered while setting up the vegetation model, including plant form, height, density, and flexibility (or stiffness). In addition to estimating resistance brought on by bed vegetation, Kubrak et al. (2008) conducted experimental tests to define channel-flow considering a free-surface layer. Referring to Huai et al. (2009), the flow in the four-rows of cylinders was created. However, the current study used periodical boundary conditions in the path of the base flow to certify the current established model. To examine the precision and precarious evaluation, the model is validated in (Figes 3 – 6 and Fig. 12), and compared against the previous researchers' work based on the different flow conditions in Table 1. Table 1 shows all the measured data from Huai et al. (2012); Run 01 and Run 09 from Lopez and Garcia (2001); Run 7 from Nepf (2012); and Run B, C, G, H, and J from Ghisalberti and Nepf (2004). It is clear that drag coefficient is very high (out of normal range) within flexible sub-merged vegetation types due to a high flexibility at the end of the stems. In this regard, the drag coefficient for rigid vegetation types within the range (low) in comparison to fully flexible vegetation types is a result of the stiffness from vegetation the stems (Aydogdu, 2023).

4. RESULTS AND DISCUSSION

This study demonstrates that the model is capable of forecasting the velocity profiles for datasets, although it has some limitations and is not perfect at forecasting.This is primarily because the vegetation layer's velocity contour formulas are insufficient. The suggested equation for computing the velocity in the upper vegetation zone requires the realising of the top and bottom velocites. As a consequence, if both of these velocities differ significantly from the measured data, the equation for the upper zone of vegetation will perform inadequately. To estimate velocity contours in sub-merged rigid vegetation, the present research contrasts the model against a considerable set of obtainable data derived from Baptist et al. (2010) and Yang and Choi (2010) who suggested various experiential models to estimate the velocity in the vegetated layer without verifing their models. The dataset comparison and the existing model are being used to exhibit the developed model's potential, which is depicted in Figs 3 to 12. These figures show that all of the model outputs can forecast contours for the vegetation at the lower-zone

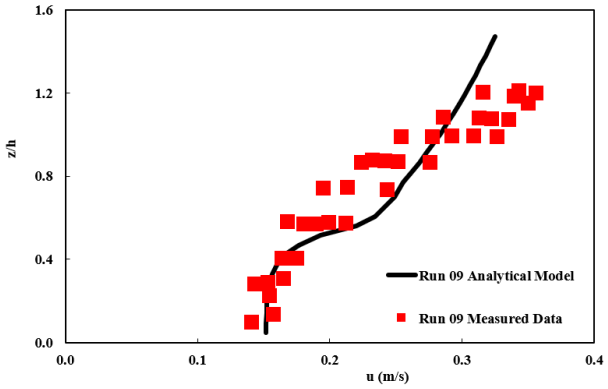

Fig. 7 Presentation of Run 09

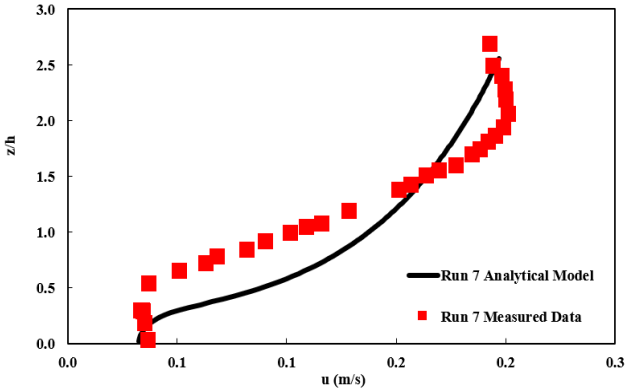

Fig. 8 Presentation of Run 7

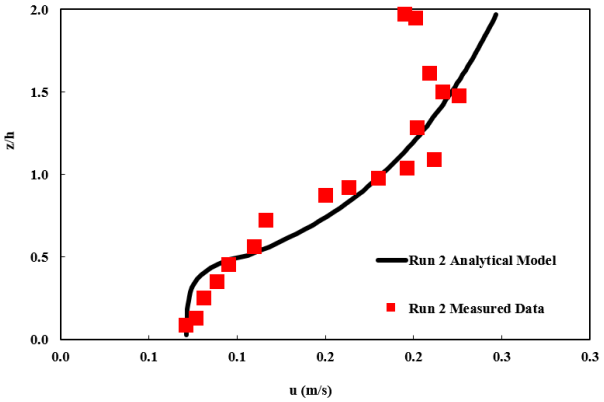

Fig. 9 Presentation of Run 2

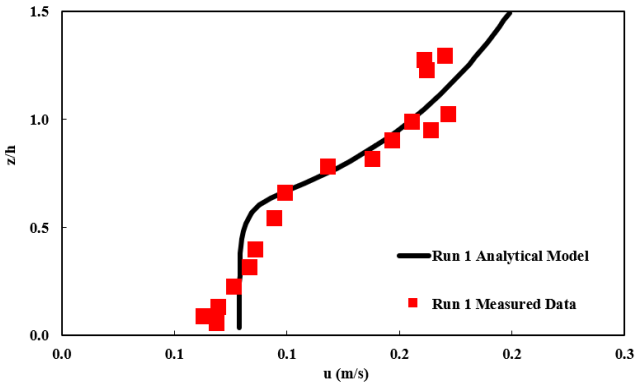

Fig. 10 Presentation of Run 1

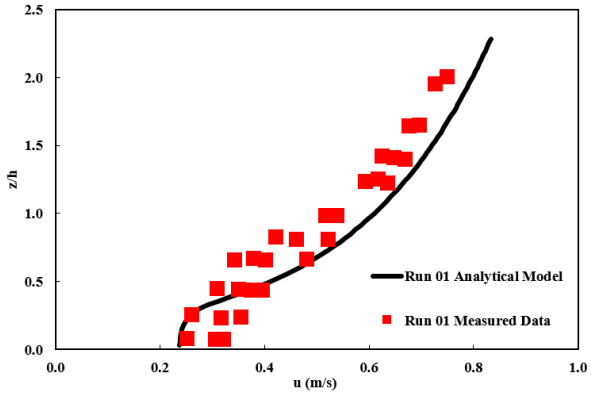

Fig. 11 Presentation of Run 01

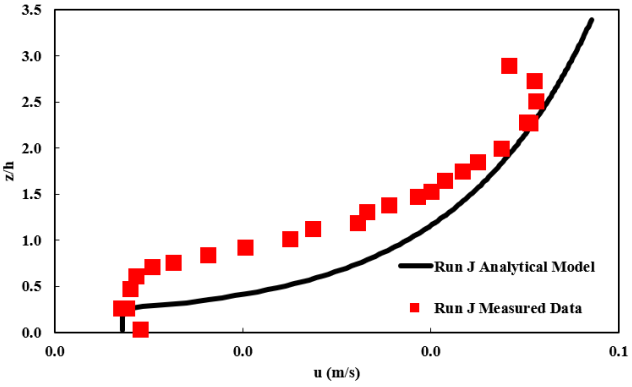

Fig. 12 Presentation of Run J

with a reasonable accuracy. Nevertheless, the velocity contour in the surface layer continues to be problematic. Specifically, this mistake is due to two things, the first of which is that the mathematical formula for the surface layer relies on the projected velocity profile in the vegetation layer. As a result, the precision of the model depends on how precisely the vegetation layer is predicted in the surface layer. Second, the analysis of the obtained data shows that there is a considerable turbulence stress penetration into the vegetation layer. In all circumstances, the velocity in the top zone is underestimated, hence the operative roughness must be significantly lesser than the height of the vegetation. Accordingly, the estimation of the top and bottom velocities of the vegetation are used in the formula provided to determine the velocity of the vegetation at the upper-zone section. As expected, the calculation of the vegetation at the upper-zone will not perform well if the top and bottom of the vegetation velocities diverge significantly from the allocated data. The specified vegetation velocity contour is exponentially represented for a significant amount of the vegetation depth in almost all of the cases examined. Furthermore, this model has occasionally predicted velocities that are extremely close to the measured data, however the pattern has not been accurately seized. This is due to the presumption that undeviating velocities has not accurately reflected the truth.

5. SIMULATED AND NUMERICAL WORK

This numerical model has been compared against the analytical results on the artificial cylinders to support the ongoing research of aquatic plants. This diffinitely would enhance flow resistance while simultaneously reducing

Table 1 Previous flexible vegetation measurements for numerical and analytical predictions

Run	1	2	1	9	B	C	G	H	J	7
Flow Discharge (m^3/s)	0.0185	0.0304	0.0179	0.058	0.0017	0.0074	0.0048	0.00143	0.0048	0.069
Channel Width (m)	0.5	0.5	0.91	0.91	0.38	0.38	0.38	0.38	0.38	0.38
Flow Depth (m)	0.29	0.38	0.34	0.21	0.46	0.46	0.46	0.46	0.46	0.44
Energy Slope (-)	0.0004	0.0004	0.0036	0.0036	0.0000018	0.000025	0.000013	0.0001	0.000013	0.0002
Vegetation Density (-)	1.57E-11	1.57E-11	1.44E-09	1.44E-09	3.61E-16	6.96E-14	1.88E-14	1.11E-12	1.88E-14	4.46E-12
Stem Diameter (m)	0.006	0.006	0.0064	0.0064	0.0064	0.0064	0.0064	0.0064	0.0064	0.0064
Vegetation Height (m)	0.19	0.19	0.12	0.12	0.139	0.139	0.138	0.138	0.138	0.16
Actual Velocity (m/s)	0.1274	0.1589	0.0587	0.2978	0.0096	0.0417	0.027	0.0806	0.027	0.4127
Submergence Ratio (-)	0.65	0.5	0.36	0.56	0.3	0.3	0.3	0.3	0.3	0.36
Stem Reynolds Number (-)	725.46	905.17	356.78	1809.68	58.21	253.1	146.16	489.54	164.75	2507.51
Developed Drag coefficient (-)	10.6	8.6	13.1	6	34.7	12	10	2	19.1	2

Table 2 Mathematical expressions to describe vegetation drag by a number of scholars

Associated method	Drag coefficient	Reference
2D RANS k-ε	1 – 1.3	Tang et al. (2014)
2D RANS k-ε	1 – 1.4	Choi and Kang (2004)
RANS k-ε	$C_D = (1000/\mathrm{Re})^{0.25}$	Huai et al. (2019)
RANS k-ε and k-ω	1.13	Huai et al. (2012)
RANS k-ε	1.0	Wilson et al. (2006)
RANS k-ω	1.13	West et al. (2016)
RANS k-ε	1.0	Swearingen and Blackwelder (2006)
Reynolds stress	1.13	Hussain et al. (2023)
RANS k-ε	1.0 – 3.0	Ghisalberti and Nepf (2004)
2D LES	2.49	Nepf (2012)
3D RANS k-ε	$C_D = 127{R_D}^{-0.572}\left(2.02\, e^{-5.91\lambda}\right)\left(0.49\, ln(h^*)\right) + 1.9$	Current study

mean velocity relative to regions without vegetation. Planning and developing flood protection systems must deliberate the interplay between the different types of vegetation and the flow characteristics (Kleeberg et al., 2010). The hydrodynamic and eco-hydraulic elements are included in the models are based on simulated scenarios that have already been researched (Lopez and Garcia, 2001; Katul et al., 2006; Luhar et al., 2008; Nepf & Ghisalberti, 2008; Perucca et al., 2009; Nikora et al., 2013). The topic of the current was alreasdy discussed in previous studies as listed in Table 2. These studies describe the velocity contour that divides the flow area into two layers within and above the vegetation layer as illustrated in the current study. A robust model to determine the average velocities and the features of turbulence flow in an open-channel with vegetation was also established by Lopez and Garcia (2001). Although this is a method for both the (Omega Model is k-ω) and (Epsilon model is k-ε) models (Table 2), the vegetation is considered both the momentum equation and the correlations of the adapted model "k-" where this is an approach. This model was developed to include flexible sub-merged types while it is utilised based on the stiff vegetation method, in addition to examining plant shape and the resistance factor concerning flow depth. Two-layer model for turbulent kinetic energy was also provided by Defina and Bixio (2005) and West et al. (2016). According to this model, vegetation both inside and above the vegetation layers considerably affected the essential variables such as the shear stress, and turbulent frequency (Cui & Neary, 2008). Table 2 demonstrates the simulation studies that were used in this study for validation by earlier researchers.

6. MODELLING AND NUMERICAL METHOD

The RANS formula in conjunction with the (k-ε) turbulent model make up the accurate framework for the

turbulent flow in the current investigation. The averaged time part and variation part are separated out for each basic flow variable.

$$\vec{U} = \vec{\bar{U}} + \vec{u} \tag{19}$$

The averaged time velocity vector is expressed in the counter of Eq. 20.

$$\vec{\bar{U}} = \frac{1}{\Delta t}\int_t^{t+T} \vec{U} dt \tag{20}$$

T is a length of time that is longer than the typical durations of the turbulent fluctuations. The RANS equations are created when mean values (in time) are used as follows;

$$\frac{\partial \rho}{\partial t} + \nabla.\left(\rho\vec{\bar{U}}\right) = 0 \tag{21}$$

$$\frac{\partial \rho\vec{\bar{U}}}{\partial t} + \nabla.\left(\rho\vec{\bar{U}} \otimes \vec{\bar{U}}\right) = \nabla.\left(\tau - \overline{\rho\vec{u} \otimes \vec{u}}\right) + \vec{S}_M \tag{22}$$

In Eq. (22), $\rho\vec{\bar{U}} \otimes \vec{\bar{U}}$ are the Reynold stressed that indicate the molecular viscosity related to stress tensor. The conservation of mass equation remains constant after adding the idea of an effective viscosity, and as a consequence, the momentum formula is given below;

$$\frac{\partial \rho\vec{\bar{U}}}{\partial t} + \nabla.\left(\rho\vec{\bar{U}} \otimes \vec{\bar{U}}\right) - \nabla.\left(\mu_{eff}\nabla\vec{\bar{U}}\right) = -\nabla p' + \nabla.\left(\mu_{eff}\nabla\vec{\bar{U}}\right)^T + \vec{b} \tag{23}$$

The effective viscosity of μeff and $\vec{b}$ is total body force for unit mass. p′ is the reformed pressure as given below;

$$p' = \rho + \frac{2}{3}\rho k + \nabla.\vec{\bar{U}}\left(\frac{2}{3}\mu_{eff} - \zeta\right) \tag{24}$$

k denotes the turbulence kinetic-energy and ζ refers to fluid bulk viscosity. This study compares (k-ε) model against (k-*ω*) to calculate the turbulence velocity contour. Specifically, the k-ε model is a 2 differential formula that considers the turbulence viscositise (μ_t) and viscosity as the summation of molecular (μ). Thus;

$$\mu_{eff} = \mu + \mu_t \tag{25}$$

At each location in the flow field, the turbulence viscosity is calculated while considering ε as the rate of turbulent kinetic energy dissipation and k as the turbulent kinetic energy as illustrated below

$$\mu_t = c_\mu\, \rho\, \frac{k^2}{\varepsilon} \tag{26}$$

$$\frac{\partial(\rho k)}{\partial t} + \nabla.\left(\rho\vec{\bar{U}}k\right) = \nabla.\left[\left(\mu + \frac{\mu_t}{\sigma_k}\right)\nabla k\right] + P_k - \rho\varepsilon \tag{27}$$

$$\frac{\partial(\rho\varepsilon)}{\partial t} + \nabla.\left(\rho\vec{\bar{U}}\varepsilon\right) = \nabla.\left[\left(\mu + \frac{\mu_t}{\sigma_\varepsilon}\right)\nabla\varepsilon\right] + \frac{\varepsilon}{k}(C_{e1}P_k - C_{e2}\rho\varepsilon) \tag{28}$$

The above equations are considered because the model for numerical cases and CFD work provides more congruence reflecting the drag-coefficient to discover the velocity contour for the specified cases as represented in the following:

Substituting $\varepsilon = \frac{\varepsilon}{k}C_\mu k_\omega$ into the dissipation formula, yields

$$\frac{\partial(\rho\omega)}{\partial t} + \nabla.\left(\rho\vec{\bar{U}}\varepsilon\right) = \nabla.\left[\left(\mu + \frac{\mu_t}{\sigma_\varepsilon}\right)\nabla\varepsilon\right] + \frac{\gamma}{\nu_t}P_k - \beta\rho\omega^2 + \left[2\,\frac{\rho\sigma\omega^2}{\omega}\nabla k{:}\,\nabla\varepsilon\right] \tag{29}$$

Compare the above equation against the k-*ω* model, yields

$$\frac{\partial(\rho\omega)}{\partial t} + \nabla.\left(\rho\vec{\bar{U}}\varepsilon\right) = \nabla.\left[\left(\mu + \frac{\mu_t}{\sigma_\varepsilon}\right)\nabla\varepsilon\right] + \frac{\gamma}{\nu_t}P_k - \beta\rho\omega^2 \tag{30}$$

Multiplication of $\left[2\,\frac{\rho\sigma\omega^2}{\omega}\nabla k{:}\,\nabla\varepsilon\right]$ by $(1 - F_1)$ and blending the (k-ε) and (k-*ω*) models results the following equations. In this regard, the transports correlations of (k-*ω*) model are included following to BST model;

$$\frac{\partial(\rho k)}{\partial t} + \nabla.\left(\rho\vec{\bar{U}}k\right) = \nabla.\left[\left(\mu + \frac{\mu_t}{\sigma_k}\right)\nabla k\right] + P_k - \rho\varepsilon \tag{31}$$

$$\frac{\partial(\rho\omega)}{\partial t} + \nabla.\left(\rho\vec{\bar{U}}\omega\right) = \nabla.\left[\left(\mu + \frac{\mu_t}{\sigma_\omega}\right)\nabla\omega\right] + \frac{\gamma}{\nu_t}P_k - \beta\rho\omega^2 + \left[2\,(1 - F_1)\,\frac{\rho\sigma\omega^2}{\omega}\nabla k{:}\,\nabla\varepsilon\right] \tag{32}$$

6.1 Model Calibration and Grid Size Independence

In-depth research and calibration are done on this model for stream wise velocity contours with vegetation stems. By putting rigid cylinders in an ordinary bed channel (Fig. 13) within the vegetation zone, different flow rates, Reynolds numbers, drag coefficients, and water flow depths are examined for the various case numbers (Swearingen & Blackwelder, 2006; Kim, 2011). The derived model is compared to the simulation results in Table 1 to ascertain whether precision increases or decreases when changing the parameters, which will change the velocity contour (McLelland & Nicholas, 2000). The recirculation length is lengthened by the horizontal distributions of averaged time velocity and time-average stream wise velocity in the re-circulation zone. The bulk drag-coefficients are unaffected by this rise. This can be attributed to the link between the bulk drag-coefficient and the reduction in the width of the wake region (Lee et al., 2004).

7. The VEGETATION MODEL

The numerical work suggested in this part, which relates to ten diverse situations, employs the analytical model to check the outcomes by a periodical length of the vegetation pattern to lessen the computing time. For numerical simulation of the flow (0.001-0.0083 m of diameter) and (a range of vegetation heights of 0.04-0.19 m) with (a range of variable flow depth between 0.0747 and 0.467 m), we have utilised 40 rigid cylinders, with the geometric measurements being derived from gathered experimental data. Plant stems were simulated as rigid cylinders of 0.49 m width, 0.3 m of flow-depth and 6.0 m of length. To accurately replicate the interplay between the flow and structure, a rigid vegetation stem has been recreated using solid cylinders (Stoesser et al., 2009). The simulation made use of a complicated mesh architecture with many elements, which has several nodes in different directions of streamwise, transverse, and vertical. According to Swearingen and Blackwelder (2006), this

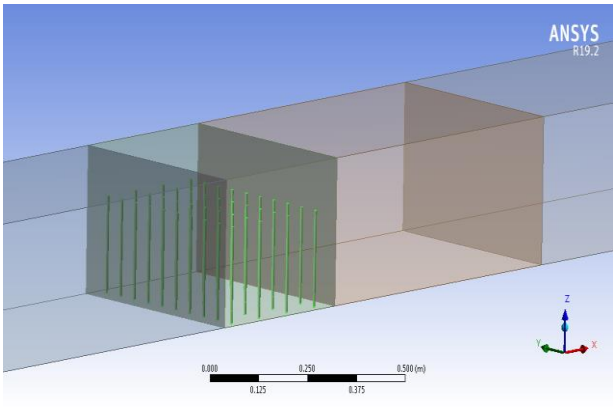

Fig. 13 The Ansys environment's 3D perspective of the vegetated channel

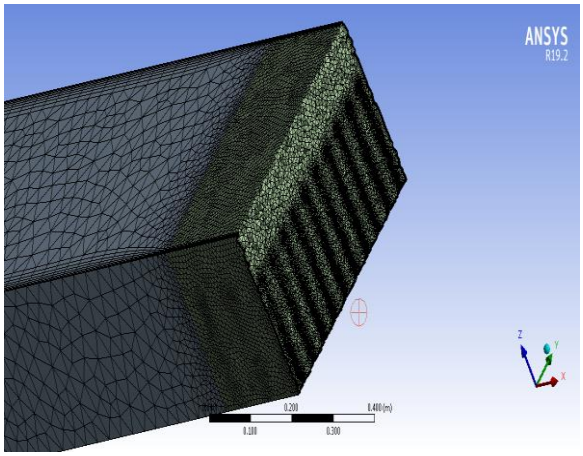

Fig. 14 The mesh produced via the Ansys-Fluent

would provid roughly square grid cells. The mesh independence test was conducted to confirm the superior quality of CFD simulation. The inlet-outlet has been used streamwise by periodical boundary-conditions that provide a contact between the faces of the inlet and outlet. The standard wall function for treating solid walls, such as the domain bed and cylinders, was used to apply the boundary condition proportionately at the free surface. The mass flowrate varies between 0.001 m^3/s to 0.2 m^3/s at the periodical border. The RANS equations were applied to a 3D simulation utilising the Ansys Fluent tool, that incorporates the finite-volume approach for spatial discretization. In the simulation, the variables of standard values were utilised because the turbulence model's short definition of the residuals' convergence requirements included them (Knight et al., 2009) and equation-governing algorithms. The length, width, and depth data from Table 1 were utilised for comparison in Ansys Fluent (the channel slope was adjusted from 0.0000018 to 0.004). Cylinders that were flexible or rigid were used to represent the plants. The vegetation density and vegetation features are expressed by the experiment parameters: (cylinder density a = 1.09 to 8 m1), (Discharge flowrate of 0.0017 m^3/s to 0.069 m^3/s), and (Fr between 0.0044 and 1.13). In this numerical work, the placement of the cylinders starts 0.15 m away from the side wall of vertical channel (Fig. 14). 40 cylinders in total were used — 10 in the first line, 10 in the second, etc.

7.1 Boundary Conditions and Mesh Design

Afree slip boundary-condition was applied to the free surface to finalise the proposed model. In Figure 13, the model's 40 cylinders positions are depicted. In a 3D perspective of the computational domain and boundary-condition, the green solid surface in the flume channel's bed, which is portrayed as 40 rigid cylinders, symbolizes the bed vegetation. The no-slip boundary condition (no-slip velocity) is deployed to the solid walls in this image. The Fluent pre-processor's mesh is seen in three dimensions. In this research, the authors used a number of mesh designs to accomplish grid independence. The mesh arrangement is an example of the selection and improvement of a sparse grid. The sensitivity to inclusive parameters, for instance mass conservation is useful in

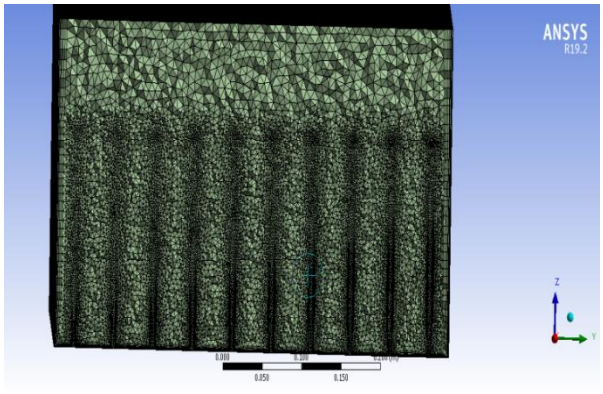

Fig. 15 Demonstration of Ansys for the produced mesh within the cylinder zone

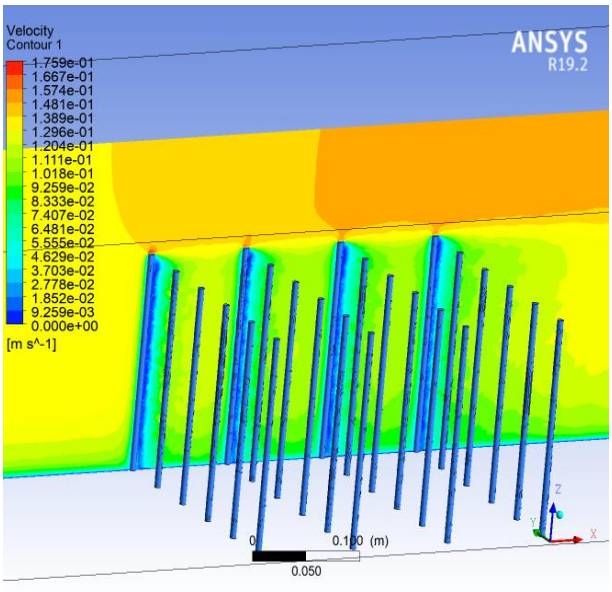

Fig. 16 Unsteady velocity distribution at initial to final stages

identifying the approximate divergence of the results while runnung the simulation instances. The simulation examples were put into practice, providing different features of the calculated 3D velocity field with mesh information in Fig. 15. Fig. 16 displays the iteration

phases for each instance, and Fig. 17 depicts the estimated velocity vector field. Each simulation instance contains a different set of elements and node numbers, and the outcome is based on a coarse grid to make the vector plot easier to read.

8. CFD SIMULATION

To verify all of the simulation cases when they vary in each run, the CFD simulation in the current research is centered around the turbulent flow type. In this regard, the specific parameters of 1000 kg/m3 of water density, 0.12 m/s of velocity, 40 cylinders, 0.006 m of cylinder's diameter, and turbulent model is (k- epsilon) were all taken into consideration utilising SST.

As shown in (Fig. 13), the x-axis is the major flow direction. This is done to numerically test how effectively imposed the periodicity requirement in the x-direction. The velocities were recorded extremely close to the solid walls, the velocity contour is substantially minor.

8.1 Mesh Arrangements

The mesh is hexagonally organized, with 4257516 elements and 7102038 nodes. The findings of the mesh run vary based on the element and node counts (Table 3). The boundaries of the inlet [symmetry, outlet, 40 cylinders, and (0) shear stress on the top and bottom walls] have been employed together with a new grid analysis to demonstrate the best mesh besides having the largest cell numbers. By utilising the mesh at various sizes and nodes, the mesh's grid sensitivity will be determined by the grid's size and resolution. Comparing the coarse, fine and standard grids have been utilised in grid dependency analysis to improve outcomes.

The turbulence velocity contour is poorly represented while the k-ω model is applied using wall functions (Erduran & Kutija, 2003). In contrast to k-ε, the k-ω model necessitates the use of an incredibly narrow grid to correctly resolution the boundary layers beyond solid wall. The shape becomes more noticeable as it gets closer to the top of the cylinder, and the vortices are visible as anticipated in the cylinder wakes. Also, it should be distinguished that at some distances, the wakes only interrelate with them very inadequately. Despite observable variations in the cylinder's bottom layer, the mesh utilised in the current experiment and the velocity profiles both revealed the same qualitative behavior.

Table 3 The design of mesh considering variable element size and nodes for the grid analysis

Number of divisions	Mesh nodes	Mesh elements
20	87451	70322
30	367811	250722
40	866361	741762
50	1676202	1038402
60	3042563	2987474
70	5823205	3989506
80	7102038	4257516
90	8152338	5249536
100	9710853	6847849

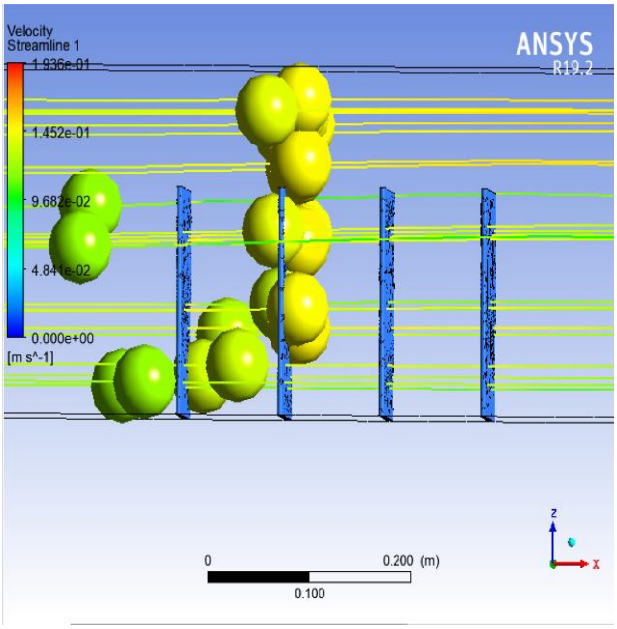

Fig. 17 Fully developed velocity profile in both layers

Despite using very small grids and a much wider computing area, Kim (2011) discovered that attaining grid independence for an identical issue was difficult. To achieve grid independence, Kim (2011) utilised profiles, which obtained the key qualitative features of the mean flow. Furthermore, no sign of convergence as the grid gets smaller was indicated. It is necessary to test for convergence when comparing the vertical velocity profiles, and this behavior can be attributed to the fact that the mass flow rate was given a number rather than having a recognised-velocity distribution defined at the computational intake of the domain. The vegetation layer poses the greatest difficulty for the flow under discussion in the context of a two/layer theoretical model, where the non-dimensional contours vary significantly (Fischer-Antze et al., 2001) (Figs 16 and 17).

9. The TEST CASES

This research utilised results from 10 diverse cases generated by simulations of different analytical models. The findings were highly promising after conducting a comparison against the experimental data. High-resolution simulations were employed to verify the RANS equations. The RANS proved accurate for rigid vegetation and extended to flexible sub-merged stems across various flow conditions. However, the model's accuracy needs further investigation for flexible vegetation types because of their intricate bending. The current research discussed changes in velocity distribution caused by the staggered arrangement and space between the cylinders. The dissipation rate of kinetic energy on the cylinders indicated small values close to the channel bottom, increasing as it moved towards the top of the cylinders.

The study utilised computational simulations through the Ansys Fluent CFD code, leading to the following conclusions:

(1) In vegetated flows, the mean streamwise velocity contours displayed a distinct variation close to the top of the vegetation layer, becoming sharper with higher initial Reynolds numbers. This sharp change was due to the interference between fast and slow flows in various layers close to the top of vegetation, creating a significant mixing layer.

(2) The average streamwise velocity considerably dropped as a result to the lack of vegetation within the vegetation layer, whereas locations with richer vegetation layouts in the upper layer had different outcomes.

(3) Flow velocities behind vegetation structures were not as accurately predicted by analytical models, a consistent finding in this study.

(4) In a comparison against upstream and downstream areas without vegetation, streamwise velocities were increased within the vegetation region. Sensitivity tests suggested the potential to decrease computational effort without sacrificing precision in predicting flows through sub-merged vegetation. However, a clear advanced turbulent closure scheme may be necessary for future research, as indicated by the challenging task of improving accuracy. The study also compared numerical and analytical models with former associated expereimntal researches (Fig. 18).

10. SIMULATION RESULTS AND DISCUSSION

The 10 simulation examples (1, 2, 01, 09, 7, B, C, G, H, and J) presented in Figs 18–27 were selected from various investigators and utilised to validate the simulation findings. As can be seen from (Figs 24 and 25), Cases 1 and 2 have similar heights of stems and space between them in the flume channel. Case 1 has less water in the flume channel than Case 2, yet Cases 1 and 2 still exhibit a distinct drag coefficient CD effect. The findings of Cases 01 and 09 are illustrated in Figs 26 and 22, respectively. Due to the different flow water rates that reach the vegetation zone in the flume channel, Case 01 exhibits greater drag coefficient than Case 09 as a result to a rise in Re number. In contrast to other cases, Case 7 has relatively little drag because there are more cylinder stems and they are spaced nearer together, as seen in (Fig. 23). The same cylinder arrangement, height, diameter, slope-gradient and flow depth are presented in Cases B, C, G, H, and J. However, the velocity profiles in these cases varied because of variable drag coefficient values relying on various vegetation densities and frontal subjected widths (Huai et al., 2013). Interstingly, the outcomes of mathematical and analytical approaches agree well with the measured velocity contours. However, as compared to the stream wise turbulent intensities, the analytical model makes accurate predictions. However, the results of mathematical model are further precise.

11. ANALYSIS OF GRID SENSITIVITY

Efficiency was considered when choosing the low-resolution grid points rather than the requirement for near-wall resolution. A grid sensitivity analysis for two simulation scenarios, both Run 1 and Run 2, has been carried out with the aim of determining if accuracy rises or declines with an increase-decrease in grid resolution. High resolution curvilinear grid is employed in the body fitted to contrust one domain Figures 18 to 27, there were a few less cells than there were when cut cells were employed. Overall, the high-resolution (Kaftori et al., 1998) prediction is well supported by the averaged time stream wise velocity distribution of all grid resolutions. The spatial averaged vertical-velocity contours are in an excellent alignment despite the velocity contour along the center-line for the nominated cylinder in the flow using a large number of grid cells. Overall, the average time stream wise velocity distribution of wholly grid resolutions provides strong provision for the high-resolution (Kaftori et al., 1998) forecast. The spatial average vertical velocity contours are in adequate alignment with the high-resolution contour despite the velocity contour alongside the centerline for nominated cylinder in the flow using a large number of grid cells. The grid resolution influences both the velocity gradients and length of recirculation zone.

The grid resolution affects the velocity gradients as well as the recirculation zone's length. Consequently, the standard mesh is the most advantageous when conducting the simulation cases, offering superior outcomes more effectively as opposed to the rest of grid sensitivities and mesh sizes at various divisions (Run 1 in Figure 28). The variation outcomes are not major due to the changes in cell size.

CONCLUSIONS

The current study intended to create a mathematical approach for calculating bulk flow velocity for both rigid and flexible vegetation under sub-merged flow circumstances. To simulate the outcomes for rigid vegetation in an open-channel with totally sub-merged vegetation, which is typical, a number of experiments were conducted. However, in reality, the findings vary depending on flexibility, especially when rigidity and flooding are taken into account. The proposed analytical model of this study founded on rigid vegetation has been modified to incorporate flexible types. The response of the bed roughness imitates to that of a fixed bed constructed from features that have been identified, geometry notwithstanding, the flexibility of the flexible parts. However, it was difficult to determine the flow resistance for flexible vegetation. As a consequence, rigid rods (cylinders) with various layouts were incorporated in the model for the present investigation. In the plant layer of submerged flows, a nearly constant velocity predominates and increases as one gets closer to the interface. The flow velocity of the surface layer is considerably greater than the one inside the vegetation layer. The findings demonstrated that plant density has a noteworthy effect on flow velocity in both emergent and submerged situations. When there is a rough sublayer present, depth-limited flow conditions over stiff vegetation may result in flow instability close to the plant interface. A vegetation-related drag coefficient was used to establish the Reynolds number-based channel shape. When designing the vegetation parameter, the effects of plant size and density

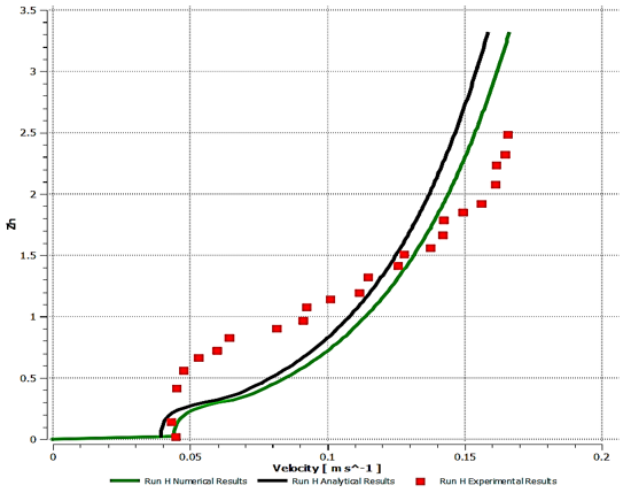

Fig. 18 Presentation of Run H

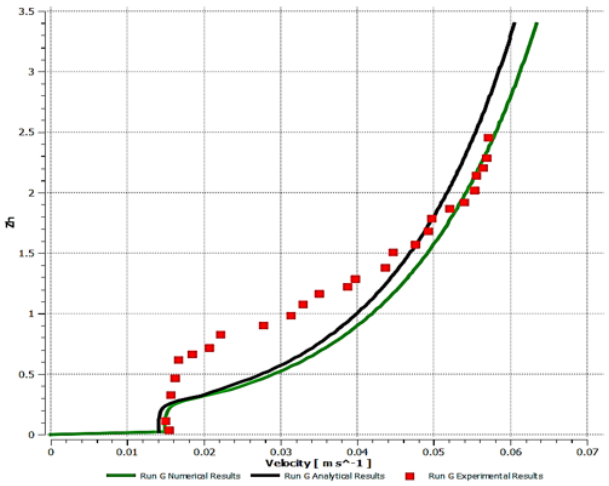

Fig. 19 Presentation of Run G

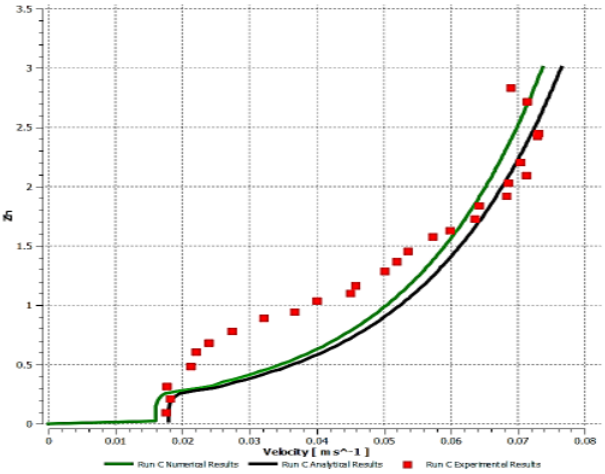

Fig. 20 Presentation of Run C

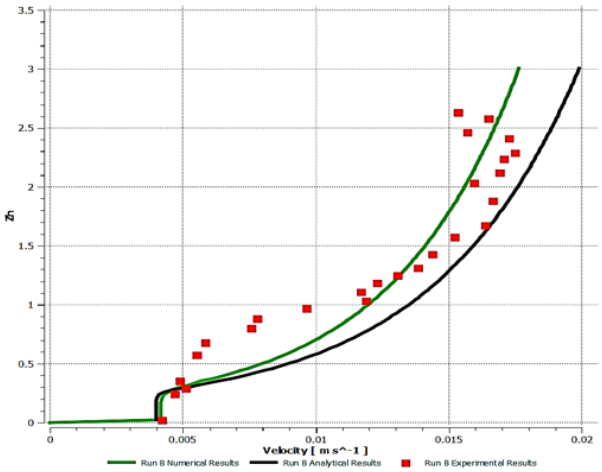

Fig. 21 Presentation of Run B

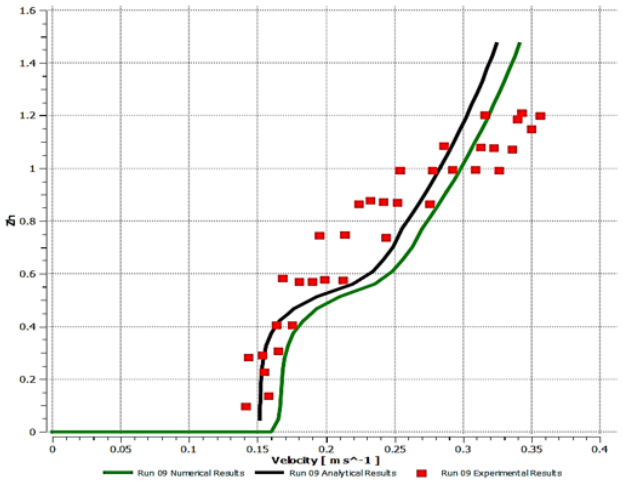

Fig. 22 Presentation of Run 09

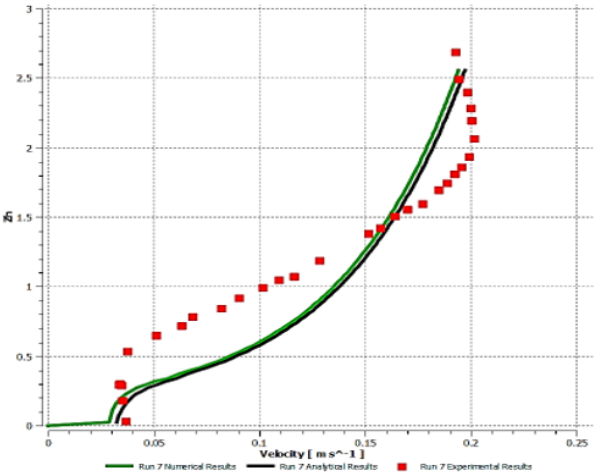

Fig. 23 Presentation of Run 7

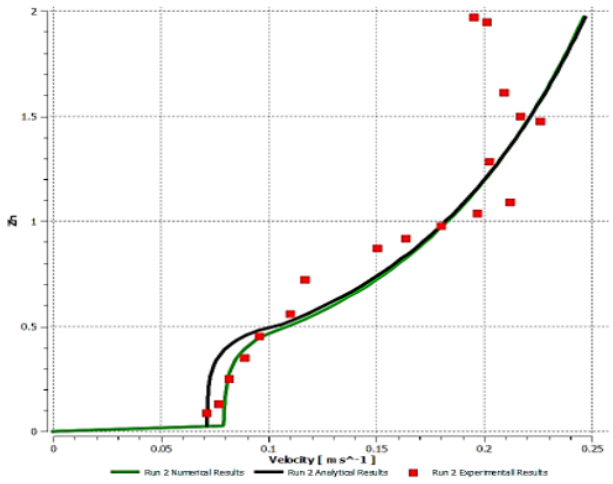

Fig. 24 Presentation of the Run 2

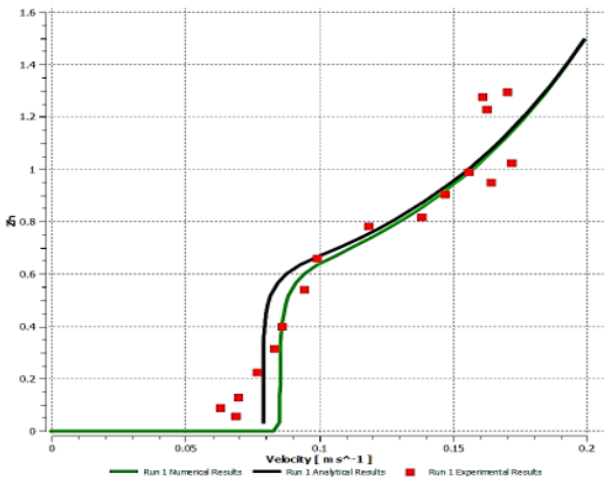

Fig. 25 Presentation of Run 1

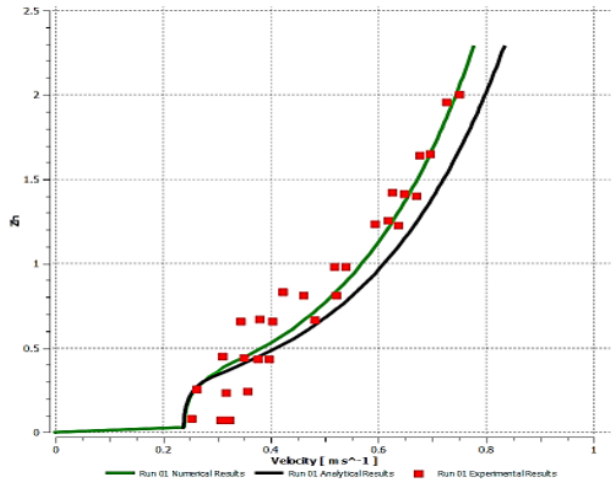

Fig. 26 Presentation of Run 01

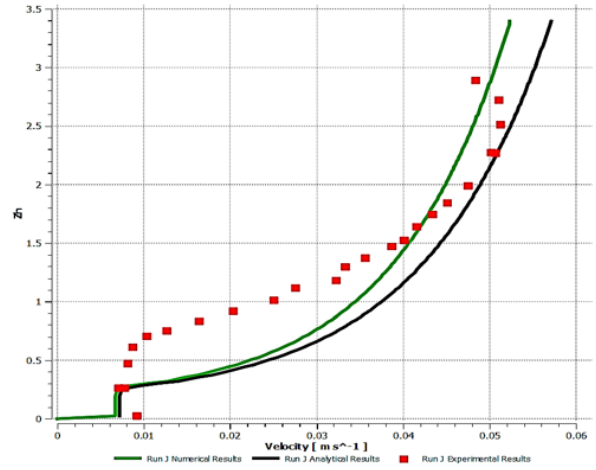

Fig. 27 Presentation of Run J

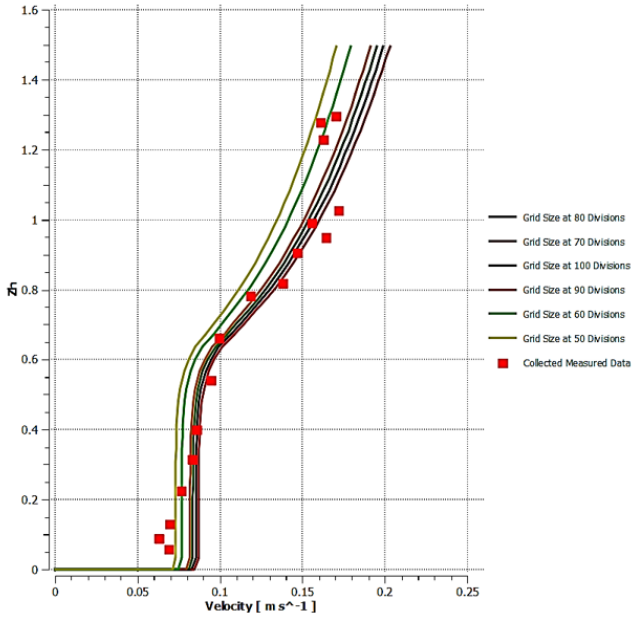

Fig. 28 Grid dependency and analysis of Run 1

were considered. To define the resistance of vegetated open-channel flows, this study developed an appropriate roughness height that takes into consideration the relative obstruction due to submerged vegetation. This analytical and numerical work revealed outstanding agreement with previously acquired measurable work that normalizes velocity contours for open-channel flows with sub-merged vegetation. The RANS simulation outcomes showed the significance of the drag coefficient (a parameter based on empirical data) for the precision of RANS simulation of flow at high-densityies' vegetation; if a greater or lesser amount of CD were depolyed, the flow resistance could be significantly overstated as the consequence of these dense levels of vegetation. It is believed that flow through submerged plant stems experiences only negligible bed friction. As a result, bed friction was taken into account when estimating drag coefficients for plants. To avoid the necessity for numerical simulation of flow through the vegetation to rely on an empirical factor, the recommended analytical model has been given and evaluated. One significant parameter that should be considered is the processing costs of various simulation approaches. With coarse grids and completely converged stable simulations, RANS simulations were run.

CONFLICT OF INTEREST

The authors declare that they have no known competing financial interests or personal relationships that could have appeared to influence the work reported in this paper.

AUTHOR CONTRIBUTIONS

Awesar A. Hussain: Conceptualization**,** methodology, software, formal analysis, writing—original draft preparation. **Mudhar A. Al-Obaidi:** investigation, writing—review and editing, supervision. **Ahmed Salih Mohammed:** software, validation, resources. **Yakubu M. John:** formal analysis, data curation. **Farhan Lafta Rashid:** investigation, visualization, supervision. All authors have read and agreed to the published version of the manuscript.

REFERENCES

Anjum, N., & Tanaka, N. (2020). Study on the flow structure around discontinued vertically layered vegetation in an open channel. *Journal of Hydrodynamics*, *32*, 454-467. https://doi.org/10.1007/s42241-019-0040-2

Aydogdu, M. (2023). Analysis of the effect of rigid vegetation patches on the hydraulics of an open channel flow with Realizable k-ε and Reynolds stress turbulence models. *Flow Measurement and Instrumentation*, *94*, 102477. https://doi.org/10.1016/j.flowmeasinst.2023.102477

Baptist, M. J., Babovic, V., Uthurburu, J., Keijzer, M, Uittenbogaard, R. E., Mynett, A., & Verwey, A. (2010). On inducing equations for vegetation resistance. *Journal of Hydraulic Research*, *45*(4), 435-450. http://dx.doi.org/10.1080/00221686.2007.9521778

Choi, S. U., & Kang, H. (2004). Reynolds stress modelling of vegetated open-channel flows. *Journal of Hydraulic Research*, *42*(1), 3-11. https://doi.org/10.1080/00221686.2004.9641178

Cui, J., & Neary, V. S. (2008). LES study of turbulent flows with submerged vegetation. *Journal of Hydraulic Research*, *46*(3), 307-316. https://doi.org/10.3826/jhr.2008.3129

Defina, A., & Bixio, A. C. (2005). Mean flow and turbulence in vegetated open channel flow. *Water Resources Research*, *41*(7). https://doi.org/10.1029/2004WR003475

Erduran, K. S., & Kutija, V. (2003). Quasi-three-dimensional numerical model for flow through flexible, rigid, submerged and non-submerged vegetation. *Journal of Hydroinformatics*, *5*(3), 189-202. https://doi.org/10.2166/hydro.2003.0015

Fischer-Antze, T., Stoesser, T., Bates, P., & Olsen, N. R. B. (2001). 3D numerical modelling of open-channel flow with submerged vegetation. *Journal of Hydraulic Research*, *39*(3), 303-310. https://doi.org/10.1080/00221680109499833

Ghisalberti, M., & Nepf, H. M. (2004). The limited growth of vegetated shear layers. *Water Resources Research*, *40*(7). https://doi.org/10.1029/2003WR002776

Huai, W., Hu, Y., Zeng, Y., & Han, J. (2012). Velocity distribution for open channel flows with suspended vegetation. *Advances in Water Resources*, *49*, 56-61. https://doi.org/10.1016/j.advwatres.2012.07.001

Huai, W., Wang, W., & Zeng, Y. (2013). Two-layer model for open channel flow with submerged flexible vegetation. *Journal of Hydraulic Research*, *51*(6), 708-718. https://doi.org/10.1080/00221686.2013.818585

Huai, W. X., Zeng, Y. H., Xu, G. Z., & Yang, Z. H. (2009). Three-layer model for vertical velocity distribution in open channel flow with submerged rigid vegetation. *Advances in Water Resources*, *32*(4), 487-492. https://doi.org/10.1016/j.advwatres.2008.11.014

Hussain, A. A., Al-Obaidi, M. A., & Rashid, F. L. (2023). Modeling of drag coefficient under emergent and submerged flexible vegetated flow. *Physics of Fluids*, *35*(6). https://doi.org/10.1063/5.0153489

Jiménez-Hornero, F. J., Giráldez, J. V., Laguna, A. M., Bennett, S. J., & Alonso, C. V. (2007). Modelling the effects of emergent vegetation on an open-channel flow using a lattice model. *International Journal for Numerical Methods in Fluids*, *55*(7), 655-672. https://doi.org/10.1002/fld.1488

Kaftori, D., Hetsroni, G., & Banerjee, S. (1998). The effect of particles on wall turbulence. *International Journal of Multiphase Flow*, *24*(3), 359-386. https://doi.org/10.1016/S0301-9322(97)00054-2

Katul, G., Poggi, D., Cava, D., & Finnigan, J. (2006). The relative importance of ejections and sweeps to

momentum transfer in the atmospheric boundary layer. *Boundary-Layer Meteorology, 120*(3), 367-375. https://doi.org/10.1007/s10546-006-9064-6

Kim, S. J. (2011). *3D numerical simulation of turbulent open-channel flow through vegetation*. (Doctoral dissertation, Georgia Institute of Technology).

Kleeberg, A., KÃHler, J. A. N., Sukhodolova, T., & Sukhodolov, A. (2010). Effects of aquatic macrophytes on organic matter deposition, resuspension and phosphorus entrainment in a lowland river. *Freshwater Biology, 55*(2), 326-345. https://doi.org/10.1111/j.1365-2427.2009.02277.x

Knight, D. W., Sterling, M., & Sharifi, S. (2009). A novel application of a multi-objective evolutionary algorithm in open channel flow modelling. *Journal of Hydroinformatics, 11*(1), 31-50. https://doi.org/10.2166/hydro.2009.033

Kubrak, E., Kubrak, J., & Rowiński, P. M. (2008). *Vertical velocity distributions through and above submerged, flexible vegetation*. *Hydrological Sciences Journal, 53*(4), 905-920. https://doi.org/10.1623/hysj.53.4.905

Kubrak, E., Kubrak, J., & Rowiński, P. M. (2012). Application of one-dimensional model to calculate water velocity distributions over elastic elements simulating Canadian waterweed plants (Elodea Canadensis). *Acta Geophysica, 61*(1), 194-210. https://doi.org/10.2478/s11600-012-0051-7

Lee, J. K., Roig, L. C., Jenter, H. L., & Visser, H. M. (2004). Drag coefficients for modeling flow through emergent vegetation in the Florida Everglades. *Ecological Engineering, 22*(4-5), 237-248. https://doi.org/10.1016/j.ecoleng.2004.05.001

Lopez, F., & Garcia, M. H. (2001). Mean flow and turbulence structure of open-channel flow through non-emergent vegetation. *Journal of Hydraulic Engineering, 127*(5), 392-402. https://doi.org/10.1061/(ASCE)0733-9429(2001)127:5(392)

Luhar, M., Rominger, J., & Nepf, H. (2008). Interaction between flow, transport and vegetation spatial structure. *Environmental Fluid Mechanics, 8*(5-6), 423-439. https://doi.org/10.1007/s10652-008-9080-9

McLelland, S. J., & Nicholas, A. P. (2000). A new method for evaluating errors in high-frequency ADV measurements. *Hydrological Processes, 14*(2), 351-366. https://doi.org/10.1002/(SICI)1099-1085(20000215)14:2%3C351::AID-HYP963%3E3.0.CO;2-K

Nepf, H. M. (2012). Flow and Transport in Regions with Aquatic Vegetation. *Annual Review of Fluid Mechanics, 44*(1), 123-142. https://doi.org/10.1146/annurev-fluid-120710-101048

Nepf, H., & Ghisalberti, M. (2008). Flow and transport in channels with submerged vegetation. *Acta Geophysica, 56*(3), 753-777. https://doi.org/10.2478/s11600-008-0017-y

Nepf, H. M., & Vivoni, E. R. (2008). Flow structure in depth-limited, vegetated flow. *Journal of Geophysical Research, 105*(C12), 28547. https://doi.org/10.1029/2000JC900145.

Nikora, N., Nikora, V., & O'Donoghue, T. (2013). Velocity Profiles in Vegetated Open-Channel Flows: Combined Effects of Multiple Mechanisms. *Journal of Hydraulic Engineering, 139*(10), 1021-1032. https://doi.org/10.1061/(ASCE)HY.1943-7900.0000779

Perucca, E., Camporeale, C., & Ridolfi, L. (2009). Estimation of the dispersion coefficient in rivers with riparian vegetation. *Advances in Water Resources, 32*(1), 78-87. https://doi.org/10.1016/j.advwatres.2008.10.007

Ren, J. T., Wu, X. F., & Zhang, T. (2021). A 3-D numerical simulation of the characteristics of open channel flows with submerged rigid vegetation. *Journal of Hydrodynamics, 33*, 833-843. https://doi.org/10.1007/s42241-021-0063-3

Rowiński, P. M., & Kubrak, J. (2002). A mixing-length model for predicting vertical velocity distribution in flows through emergent vegetation. *Hydrological Sciences Journal, 47*(6), 893-904. https://doi.org/10.1080/02626660209492998

Stoesser, T., Salvador, G. P., Rodi, W., & Diplas, P. (2009). Large Eddy Simulation of Turbulent Flow Through Submerged Vegetation. *Transport in Porous Media, 78*(3), 347-365. https://doi.org/10.1007/s11242-009-9371-8

Swearingen, J. D., & Blackwelder, R. F. (2006). The growth and breakdown of streamwise vortices in the presence of a wall. *Journal of Fluid Mechanics, 182*(-1). https://doi.org/10.1017/S0022112087002337.

Tang, H., Tian, Z., Yan, J., & Yuan, S. (2014). Determining drag coefficients and their application in modelling of turbulent flow with submerged vegetation. *Advances in Water Resources, 69*, 134-145. https://doi.org/10.1016/j.advwatres.2014.04.006

Tsujimoto, T., & Kitamura, T. (1990). Velocity profile of flow in vegetated-bed channels. *KHL Progressive Report, 1*, 43-55.

West, P., Hart, j., Guymer, I., & Stovin, V. (2016). Development of a laboratory system and 2D routing analysis to determine solute mixing within aquatic vegetation. *Hydrodynamic and Mass Transport at Freshwater Aquatic Interfaces*, 49-61. http://dx.doi.org/10.1007/978-3-319-27750-9_5

Wilson, C. A. M. E., Yagci, O., Rauch, H. P., & Olsen, N. R. B. (2006). 3D numerical modelling of a willow vegetated river/floodplain system. *Journal of hydrology, 327*(1-2), 13-21. https://doi.org/10.1016/j.jhydrol.2005.11.027

Yang, W., & Choi, S. U. (2010). A two-layer approach for depth-limited open-channel flows with submerged vegetation. *Journal of Hydraulic Research, 48*(4), 466-475. https://doi.org/10.1080/00221686.2010.491649